A Landmark Based Pinpoint Landing Simulator

Yang Cheng, Adnan Ansar,
Mobility Systems Concept Development Section
Jet Propulsion Laboratory, California Institute of Technology
4800 Oak Grove Drive, Pasadena, CA 91109-8099, USA
Phone: 818-354-1857 Fax: 818-394-4085
Email: ycheng@telerobotics.jpl.nasa.gov

Key Word: Pinpoint landing, Landmark Detection, Crater Matching, Position Estimation.

Abstract
Real-time position estimation for a descent lander is a critical technological need for many planned NASA missions. In particular, it enables the ability to land precisely and safely in a scientifically promising but hazardous site and is a key technology to be demonstrated by NASA in the next decade. The primary question of pinpoint landing is how to localize the lander by recognizing landmarks (craters) in the landing area and match them positively to a preexisting landmark database while the spacecraft is descending. In addition, there are several equally important operational issues. For example, what is the optimal field of view (FOV) of the descent camera to ensure maximum chance of success? What accuracy can the pinpoint landing approach achieve? How many landmarks are needed to ensure unambiguous localization? What is the performance requirement of each individual algorithm involved (the crater detection rate, the false alarm rate, ant the crater position error, speed, *etc*.)? In order to answer these questions, a **la**nd**m**ark-based **p**inpoint-landing **s**imulator (LAMPS) is under development. The current LAMPS can conduct two types of assessment: a position accuracy analysis and a crater constellation uniqueness analysis. The results are very valuable for pinpoint landing related R&D as well as mission design and planning. Finally, a case study of a hypothetical landing scenario is given.

Introduction
Craters are landforms commonly found on the surface of planets, satellites, asteroids, and other solar system bodies. A crater, in general, is a bowl shaped depression created by collision or volcanic activities. Because of their different geological ages and magnitudes of impact, craters may have a wide range of appearances. For instance, younger craters may have sharper and regular rims while aged craters may have very vague rims. Spatial densities of craters also form the primary basis for assessing the relative and absolute ages of geological units on planetary surfaces. However, a typical crater in an image has an elliptical rim and a bright to dark shading pattern, which is dictated by the lighting azimuth and elevation as well as its own topography.

Because of their simple and unique geometry, craters are ideal landmarks for spacecraft navigation [2-5]. Optical landmark navigation using craters on the surface of a central body was first used operationally by the Near Earth Asteroid Rendezvous (NEAR) mission [4-5]. It has been shown to be a powerful data type for determining spacecraft orbits about the body for close flybys and low attitude orbiting. In the navigation filter, detected and identified craters were combined with Deep Space Network (DSN) radiometric tracking (Doppler and range) to estimate both orbital and asteroid physical parameters. The crater locations were also estimated. The direct benefit of optical landmarks in NEAR navigation has been enhanced navigation performance, specifically in increase in orbital position accuracy to 10 - 20 meter range, faster estimate convergence after maneuvers, and better solutions for dynamical parameters, such as spacecraft non-gravitational accelerations and Eros gravity perturbations. Another benefit of using landmark tracking has been the rapid determination of poorly known physical parameters of Eros which affect navigation, such as spin pole direction and spin state.

Another important use for landmarks is spacecraft pinpoint landing (PPL). The current Entry, Descent and Landing (EDL) capability has a very large landing error ellipse. The landing ellipses for the Viking landers, Mars Pathfinder, Mars Polar Lander, and Mars Exploration Rovers have a semi-

major axis on the order of 100-300 km. Guided entry is expected to shrink the landing ellipse to 3-6 km for second-generation landers as early as 2009. However, even if a landing ellipse is only a few kilometers in size, it is very likely to contain hazards such as craters, steep slopes, and rocks, regardless of how the ellipse is selected. To decrease the probability of landing on a hazard, one of two safe landing approaches may be employed: crater hazard detection avoidance, which will detect all hazard craters during the descent and avoid landing inside any of these craters, or pinpoint landing, which determines the lander's position in real-time and guides the spacecraft to land at a pre-selected site. According to recent studies on the size/frequency of craters on the surface of Mars [7], a sufficient number of adequately sized craters for determining spacecraft position are very likely to be found in descent imagery. For example, if an image is taken at 8km above the surface with 45-degree camera Field of View (FOV), there will be an average of 94 craters of < 200 m diameter in the image. These craters can be used as landmarks to match a pre-existing crater database and, therefore, to determine the position of the lander.

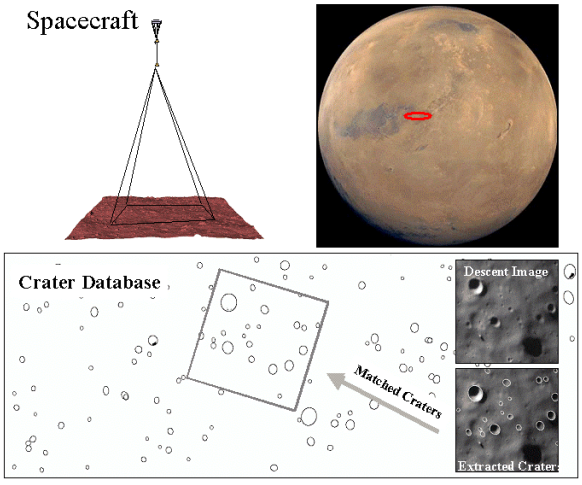

Figure 1: Craters in the descent image are identified and matched to a database. Using the known 3D positions of the craters and their 2D images, the position and attitude of the lander can be computed in real-time during descent**.**

PPL Operation Scenario and Requirements

The landmark-based pinpoint landing approach is as follows. First, a scientifically interesting landing site on the targeted body is selected on earth using orbital imagery, and the landmarks (e.g. craters) within the landing ellipse are mapped. During the lander descent, its initial position with respect to the landmarks as well as to the selected landing site is determined automatically on board. The lander is then guided to the landing site using continuous updates of lander position and velocity throughout the descent (Fig. 1). Three key algorithms enabling PPL are the landmark (crater) detection, landmark matching, and position estimation.

Crater Detection

A very robust crater detection algorithm has been developed for autonomous spacecraft navigation [2]. After some modification, this algorithm can be used for PPL as well. The crater detection algorithm consists of five individual steps.

1. Edge Detection: This step detects edges in an image and places them in a database.
2. Rim Edge Grouping: This step groups together edges that belong to the same crater. The information used for this process include edge shape (convex), the image intensity profile inside a crater, and edge gradients. If a pair of edges (lit and shaded side of crater) is found, they will be used to fit an ellipse.
3. Ellipse Fitting: This step fits an ellipse to each group of crater edges by an iterative algorithm – the reweighting least square method, which can robustly remove any outliers in the input points.
4. Precision Fitting: This step adjusts the detected crater's geometry directly in the image domain to reduce errors introduced in edge detection and ellipse fitting. A multidimensional iterative nonlinear minimization algorithm based on conjugate gradients is used to lock an ellipse precisely on the rim of a crater.
5. Crater Confidence Evaluation: This step evaluates every detected crater and assigns a confidence value to it.

An extensive experimental study shown that the detection rate is better than 94% and the false alarm rate is less than 7%. The position error is less than 0.3 pixel and the geometrical error is less than 0.5 pixel. Fig.2 shows two results of the crater detection algorithm. The left side is a NEAR Eros image and right side is a Mars Odyssey image

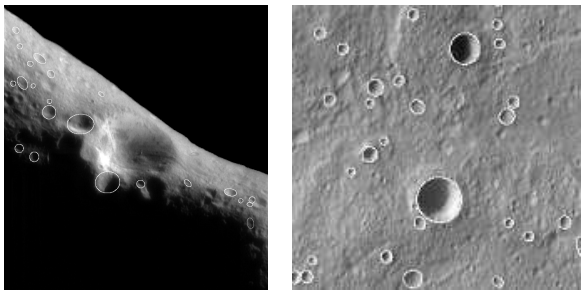

Figure 2: Two examples of crater detections

Crater Matching

In order to determine the position of the spacecraft with respect to the central body, geometrical recognition techniques that perform matching between the craters that have been extracted from an image and a crater database containing the 3D locations of the craters, is used here. Each crater is treated as an attributed point corresponding to the center of the crater, where the attributes are the radius and orientation of the crater. The efficiency of the basic methodology is improved by two means. First, the crater attributes are used to remove matches that are incompatible. Second, an initial estimate of the spacecraft position is used to filter matches that are not feasible. Besides, the information from other sensor such as the altitude from the altimeter and attitude from the IMU can help to reduce the search scope even more.

Position Estimation

From a suitable number of matched landmarks for which we have prior geometric data, we accurately estimate the position and orientation of the spacecraft with respect to the surface of the planetary body. In the case of craters, the relevant structures are crater centroids, which are estimated carefully to account for perspective distortion effects.

Given a collection of points in 3D and their 2D projections, we recover camera pose as follows. The 3D points are originally presented with respect to some reference coordinate frame, typically dependent on the landing ellipse and independent of the location of the camera. The first step in recovering camera pose is to determine the coordinates of these points in a coordinate frame centered on the camera. From prior calibration of the camera, we know the exact 2D coordinates of a pixel on the image plane (CCD or CMOS device). If *(x,y)* are the 2D coordinates of an image point *p* arising from a 3D point *P*, then *P* can be expressesfigure in the coordinate frame of the camera as $(\lambda x, \lambda y, \lambda)$ for some suitable scale factor λ. Note that the distances between 3D points are independent of coordinate system. Hence, for a collection of image points $\{p_i\}$ and associated 3D points $\{P_i\}$, we know $\{d_{ij}=\|P_i-P_j\|\}$. This can be expressed as

$$d_{ij}^{\ 2} = (\lambda_i x_i - \lambda_j x_j)^2 + (\lambda_i y_i - \lambda_j y_j)^2 + (\lambda_i z_i - \lambda_j z_j)^2$$

resulting in a set of quadratic equations in the unknown $\{\lambda_\iota\}$. We use an efficient and robust linear algorithm to solve for the λ_ι[8]. Once these quantities are known, the 3D coordinates of all points are known in both the coordinate frame of the camera and the reference frame. Recovery of the camera pose is then equivalent to finding the Euclidean transformation, which maps one of these point clouds onto the other. This absolute orientation problem has a known optimal solution [8]. For small numbers of points, it is fast and very robust. It requires no initialization because there is no iterative component. Consequently, there are no convergence or local minima issues.

The PPL scenarios and requirements differ significantly from mission to mission. For example, landing on a large planetary body, such as Mars, the PPL will start only after the heat shield is jettisoned, where the lander is already very close to final touch down and is descending very rapidly (~100m/s). Because of high vertical velocity and short travel distance, an ultra fast PPL is needed. In order to achieve this, valid options include use of very efficient algorithms, reduction of the data volume and use of faster computers. For example, using the smallest number of craters possible without ambiguity in PPL could save significant processing time. However, what is the minimum number of craters to ensure unambiguous localization? What is the effect on the position accuracy if few craters are used in PPL?

Computationally it is more feasible to do PPL on a small body than on a large body because of its lower gravity and consequentially lower descent velocity. However, since most small bodies have irregular shapes, unique challenges remain. For example, the craters appear differently due to the view and lighting angles and local surface normals, and the plane assumption for large bodies is no longer valid. This may create some difficulties in

crater matching. Another problem with small body PPL is that the portion of covered area might be on the dark side of the body(Fig.2). So only a small fraction of craters appear in a descent image. In this case, the crater detection rate is much lower than on a large body. For small body landing, we need to answer the following questions: What is the minimum detection rate? Where and when the PPL is feasible? What is the optimal FOV? Do we need a second descent camera with small FOV to compensate for the range limitation of wider FOV cameras? Not all these questions can be addressed analytically. However, a well-designed and high fidelity simulation can provide much insight.

LAMPS

In order to answer these questions above, a **la**nd**m**ark-based **p**inpoint-landing **s**imulator (LAMPS) is being developed. The objective of LAMPS is to provide solid answers to many operational questions. LAMPS can incorporate numerous types of information and data to simulate a real mission scenario (Fig.3).

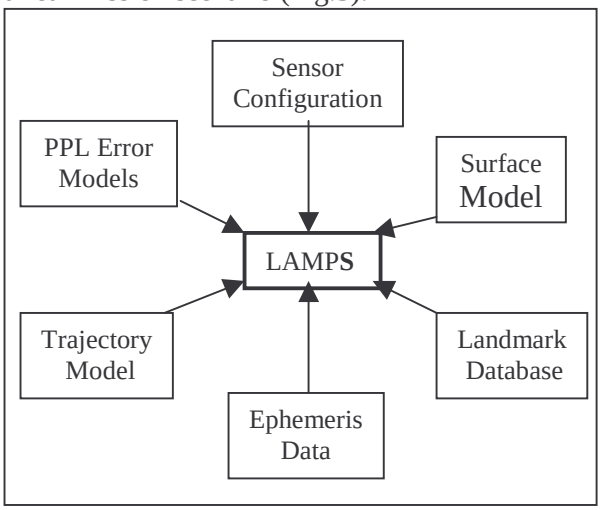

Figure 3. The framework of LAMPS

The input data that LAMPS will use include

1. PPL error models, which include error models of each individual algorithm involved, such as the landmark detection rate, false alarm rate, landmark position and geometry error, etc.
2. Surface model: When the local surface is not flat, which is particularly true for small bodies, a local surface model will play an important role in the landmark appearance in the optical image.
3. Landmark database, which includes the position, major and minor axes, orientation, and local surface normals, etc. of all craters.
4. Spacecraft trajectory: which includes the trajectory error models, such as error ellipse,
5. Sensor error model: Sensor's error model, Attitude error of IMU, range error from range finder, camera calibration model.
6. Ephemeris data: sun position, central target's attitude etc.

Currently, LAMPS can perform two types of analysis: the position estimation accuracy analysis and crater constellation uniqueness analysis.

Crater Constellation Uniqueness Analysis

To be used for unambiguous position estimation, the constellation of landmarks must be unique in terms of size and location in the landing ellipse. Our initial study uses the Odyssey THEMIS data mentioned above, which contains 917 detected craters. We detect for all clusters of 3 to 10 points within the chosen FOV of the camera in any initial position, whether there is a rigid motion taking the given cluster to another. In such a case, position estimation will be inherently ambiguous if these craters are chosen for the estimate. Note that our analysis is exhaustive in the sense that we examine all 270,000+ admissible configurations of 3 craters. Since, any ambiguous constellation n>3 craters is also ambiguous for subsets containing 3, the associated rigid motion for the n crater case is covered by our analysis.

Position Estimation Analysis

From a suitable number of matched landmarks for which we have prior geometric data, we accurately estimate the position and orientation of the spacecraft with respect to the surface of the planetary body. We identify 3D to 2D point correspondences between our database and descent or orbital imagery. In the case of craters, the relevant structures are crater centroids, which is estimated carefully to account for perspective distortion effects. We study this accuracy of this approach via a detailed simulation described below.

Given a dataset containing the 3D locations of crater centroids within a theoretical landing ellipse, we randomly insert the spacecraft within the ellipse assuming a truncated Gaussian distribution with σ_x and σ_y derived from the major and minor axes. By truncated, we mean that we do no allow insertion

outside the landing ellipse. We set insertion altitude, orientation, imager resolution and FOV as desired. The onboard camera then takes a virtual snapshot of the visible portion of the 3D terrain. The 2D image coordinates of the crater centroids are distorted noise with a truncated Gaussian distribution with predefined standard deviation and truncation point. If there are not enough craters (a tunable parameter *n* with a minimum value of 4) for position estimation, we mark the insertion point as a failure. Otherwise, we randomly select *n* of the visible craters for position estimation. Assuming perfect matching between the 2D and 3D datasets, we use our position estimation algorithm to estimate spacecraft position and orientation and compare to the preset ground truth. In our initial version of this simulation, we are not doing any form of temporal averaging. Therefore, results are on a frame-by-frame basis. We are also ignoring the fact that with a laser altimeter and knowledge of the gravity vector the pose problem becomes much better constrained and the remaining degrees of freedom can be more accurately estimated.

Case Study

We now present a case study of both the position estimation and constellation uniqueness analysis using imagery of a 24km x 45km patch of the Martian surface taken from the Odyssey THEMIS mission. In Fig.4, we see the actual image (warped) along with a crater density map.

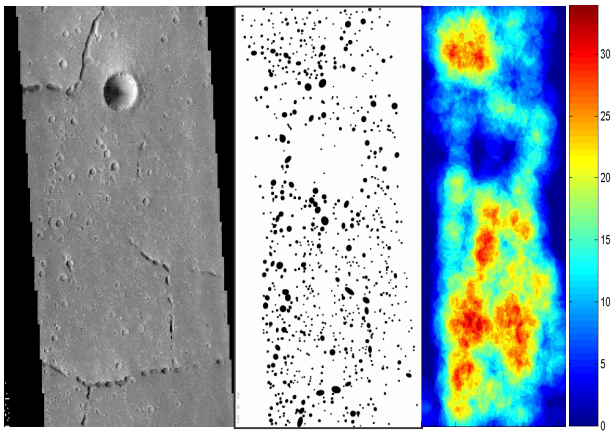

Figure 4. Oddysey THEMIS image (left). Detected craters (center). Crater density map (right)

For the uniqueness analysis, we chose a FOV of 45 degrees, an altitude of 8km and a downward looking camera. Note that this resulted in over 270,000 unique clusters of 3 points within the FOV ranging over all initial positions. Two clusters were considered identical there existed a rigid motion taking one to other, subject to error bounds. In particular, we required the major and minor axes of

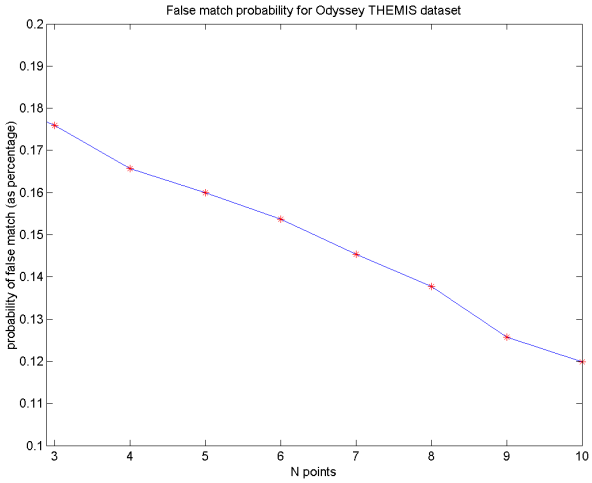

Figure 5. Probability of ambiguous configuration for n=3 to 10 points.

related ellipses to vary by no more than 5 meters and the crater centers to vary by no more than 50 meters. In practice, these are highly conservative numbers. In Fig.5, we show the percentage probability of finding an ambiguous constellation, given n points in the constellation with the camera FOV, where n ranges from 3 to 10. With the small number of craters in our dataset, even the case of 3 points is ambiguous in <0.2% of cases. In particular, since we prune by crater shape, the set of viable candidates decreases dramatically. We are currently working on other datasets and on extending our result to a purely analytical model, which depends only on crater density and error models rather than on a set of crater data.

The simulation framework for all position estimation analyses to follow is as described above with the following parameters: altitude = 8 km., orientation = downward pointing, image resolution = 1024 x 1024. In figure 6 we plot for 3 different FOVs and 50000 insertion points each, the areas over which 5 craters are visible. As we will show, 5 craters appear adequate for the position estimate.

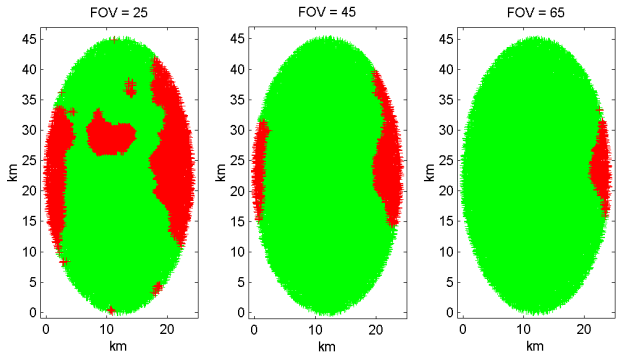

Figure 6. Success (in green) vs. failure (in red) for insertion 50000 positions and 25 deg (left), 45 deg (center) and 65 deg (right) FOV.

Note that with low depth variation (there is none at all in our case), position estimation is least accurate along the viewing direction (downward in our case). However, in a real implementation, we would have highly accurate estimates of elevation and gravity vector from other onboard systems. This not only constrains the most sensitive component of our estimate but also reduces the number of degrees of freedom of the search. In our current implementation, we do not take this extra information into account. We would use a state estimator and temporal filtering to stabilize the pose estimate in a real-world system. In the current version of the simulation, we estimate pose from single frames only. Hence, as a measure of consistency, we take two estimates for each insertion position, using different subsets of points and different random noise. If the recovered positions and attitudes differ by more than 100 meters or 10 degrees, we reject the data as an outlier. Note that this is very conservative, since an altimeter would reduce the elevation error dramatically. This interim procedure will be replaced by a state estimator and planned trajectory approach in subsequent versions. Below, we vary FOV by increments of 5 degrees from 20 to 90. For each angle we perform 5000 random insertions as described above using 5 points for position estimation with noise set to σ=0.5 pixel. The results are shown in Fig.7.

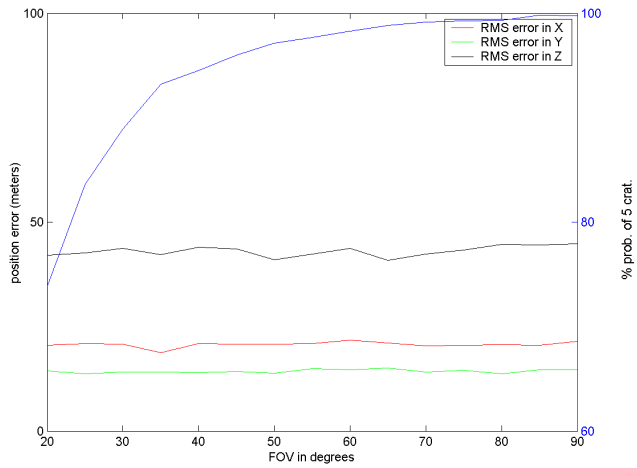

Figure 7. RMS position error in X (red), Y(green) and Z(black) for FOV ranging from 20 deg. To 90 deg. Probability of finding 5 craters in blue.

As expected, the recovered position estimate in the Z (camera depth and spacecraft elevation) direction is the worst. However, the lateral position estimate is on the order of 20 meters at an altitude of 8 km. We find this result very encouraging. The error appears to be largely independent of FOV with the given camera configurations. Observe that the probability of finding the requisite number of craters increases with FOV. Further study is warranted, but this result seems to indicate that within limits defined by resolution, etc., the largest FOV is preferable for position estimation

Conclusions

In this paper, LAMPS is presented. This system can incorporate many types of information to simulate a real operational scenario. LAMPS can answers many operational questions, which are often very important but hard to address analytically. In short, it is a very valuable tool in PPL research and development and PPL mission design and planning.

Future work on the LAMPS will include incorporating the surface model, spacecraft trajectory model, and ephemeris data into the system.

Acknowledgments

The research described in this paper was carried out at the Jet Propulsion Laboratory, California Institute of Technology, under a contract with the National Aeronautics and Space Administration.

References

[1] Ed Wong, “Hazard detection and avoidance: Lander operating conditions”

[2] Yang Cheng, A. Johnson, C. Olson, L. Matthes, “Optical Landmark Detection for Spacecraft Navigation” 13th Annual AAS/AIAA Space Flight Mechanics Meeting.

[3] Yang Cheng, James Miller “Autonomous landmark Based Spacecraft Navigation”, 13th Annual AAS/AIAA Space Flight Mechanics Meeting.

[4] B. Williams, J.K. et al. “Navigation Results for NASA’s Near Earth Asteroid Rendezvous Mission, AIAA/AAS Astrodynamics Specialists Conference.

[5] J. K. Miller et al “Determination of Shape, Gravity, and Rotational State of Asteroid 433 Eros”, *Icarus* 155 3-17 (2002).

[6] David Forsyth et all, “Invariant descriptors for 3-D object recognition and pose” *IEEE PAMI*, Vol. 13, No. 10, 1991.

[7] Gouglas Bernard and Matthew Golombek, “Crater and rockhazard modeling for Mars Landing”, AIAA Space 2001 conference, Albuquerque, NM.

[8] Adnan Ansar, Kostas Daniilidis “Linear Pose Estimation from Points or Lines”, *IEEE PAMI*, 2003, to appear .

[9] B.K.P. Horn, et al., “Closed-form Solution of Absolute Orientation Using Orthonormal Matrices,” Journal Opt. Soc. Am. A, A5: 1127-1135, 1988.